

## Polarization observations of broadband VHF signals by the FORTE satellite

Xuan-Min Shao and Abram R. Jacobson

Space and Atmospheric Sciences Group, Los Alamos National Laboratory, Los Alamos, New Mexico, USA

**Abstract.** Coherent very high frequency (VHF) radio observations with the pair of orthogonal log-periodic array antennas of the FORTE satellite allow us to study thoroughly the polarization properties for a received signal. Eighty-one broadband VHF pulses that were generated by the Los Alamos Portable Pulser (LAPP) have been analyzed. The data are analyzed by computing the Stokes parameters in the time-frequency domain. We first examine the LAPP pulses at high time resolution so as to separate the ordinary and extraordinary ionospheric modes. The two modes have been found to be mirror images of each other in terms of polarization, as would be expected. For each mode the polarization degrades from circular toward elliptical as the nadir angle increases. Antenna pattern effects on this observation are discussed. The tilt of the detected polarization ellipse is found to be tightly associated with the azimuthal direction of the pulse source. The same set of data are then examined with much lower time resolution to intentionally mix together the two split modes, so that the ionospheric Faraday rotation can be detected. With the known geomagnetic field the total electron content (TEC) is computed, which shows good agreement with the TEC computed by dechirping the signal. A case study of an impulsive lightning emission shows that it is highly polarized, indicating that the associated breakdown processes are highly coherent and organized. Finally, we discuss the potential use of the polarization observations for locating terrestrial radio signals.

### 1. Introduction

The FORTE (Fast On-Orbit Recording of Transient Events) satellite was launched on August 29, 1997 into a 70° inclination, nearly circular orbit at 800 km altitude. The satellite carries two broadband log-periodic dipole array antennas (LPA) that are orthogonal to each other along the same boom pointing to the satellite nadir. The antennas are connected to two separate radio receivers that have a bandwidth of 22 MHz with their center frequency tunable between 20 and 300 MHz. Under one of FORTE's several radio operation modes the two receivers are placed in the same frequency band and are phase-synchronized. This configuration allows thorough investigations of the polarization properties for the received radio frequency signals.

A radio signal that propagates from the Earth to the FORTE satellite will pass through the Earth's ionosphere below 800 km altitude. The signal will be split into the "ordinary" and "extraordinary" modes by the coupled effect of the ionosphere plasma and the Earth's magnetic field [Budden, 1985; Davies, 1990]. The two modes of the signal will propagate independently along slightly different paths with different phase and group velocities. For a linearly polarized VHF signal the two corresponding modes will share about the same radiation power, and each of the modes will be nearly circularly polarized with the electric field vector ( $\mathbf{E}$  vector) rotating one way for the ordinary mode and the opposite way for the extraordinary mode. For an impulsive signal the two modes may or may not overlap temporally at the point of the FORTE satellite, depending on the frequency examined, the total electron content (TEC) the signal traversed, and the dot-product of the wave normal and the magnetic field vectors [Massey *et al.*, 1998]. In the case of the two modes being separated temporally, signal properties associated with the power and

Copyright 2001 by the American Geophysical Union.

Paper number 2000RS002600.  
0048-6604/01/2000RS002600\$11.00

polarization for each of the two individual modes can be observed. In the case where the two modes couple together, the two nearly circularly polarized modes will result in a nearly linearly polarized wave, closely resembling the linearly polarized wave originally emitted from the ground. However, as contrasted to the free space wave propagation, the E vector of the linearly polarized wave will rotate continuously while passing through the ionosphere, a phenomenon called Faraday rotation. For a given path between the radio source and the satellite the total number of Faraday rotations depends on the frequency ( $\propto f^{-2}$ ). For a broadband signal the relative amount of rotation between different frequency components can be observed.

Polarization studies of transionospheric VHF signals have been reported by many researchers previously, as reviewed by *Davies* [1980]. The previous studies have focused on the Faraday rotations for a single frequency or multiple narrowband VHF signals from satellite radio beacons that were often transmitted continuously, so that the TEC and ionospheric disturbances would be monitored. Satellite observations of broadband VHF dispersion, magnetoionic splitting, and mode beating have been presented more recently by *Holden et al.* [1995], *Massey et al.* [1998], *Jacobson et al.* [1999], and *Jacobson and Shao* [2001]. Most of these works have been conducted at Los Alamos National Laboratory by using the broadband RF payloads on the ALEXIS and FORTE satellites.

In this paper, we present the FORTE polarization observations of broadband VHF signals by coherently analyzing the signals received by the two crossed LPA antennas. The broadband signals were produced by an electromagnetic pulse generator named Los Alamos Portable Pulser (LAPP), located at Los Alamos, New Mexico (35.87°N, 106.33°W). We will also present a case study for lightning-produced pulses to show the usefulness of the polarization observations for lightning investigations.

## 2. FORTE RF Antennas and Radio Receivers

The FORTE RF antenna consists of a pair of identical LPA antennas that are mounted orthogonally to each other along a 10 m boom pointing to the satellite nadir. One LPA is aligned in the direction of

the satellite trajectory, and the other is in the direction orthogonal to the trajectory. Each LPA has 10 dipole elements along the boom with the longest and shortest dipoles being half wavelengths at 30 and 90 MHz, respectively. The primary operating frequencies of the antennas are therefore between 30 and 90 MHz. With such a structural configuration each LPA has a directivity gain of  $\sim 5$  dBi (relative to an isotropic antenna) at the middle of its operating frequencies. The corresponding half-power beam width is  $\sim 60^\circ$  in its E plane and is about  $210^\circ$  in its H plane. The first null in the E plane lies at  $\sim 60^\circ$  from the nadir so that the main lobe of the antenna matches the field of view from the satellite to the Earth. (At 800 km altitude the limb of the Earth is  $\sim 60^\circ$  from the nadir direction.)

In addition to the normal capabilities of a LPA antenna the FORTE antennas were designed also to operate at higher-frequency modes. Each antenna element was pitched  $20^\circ$  toward the nadir direction to form a V-shaped dipole, so that at frequencies  $3/2$  of the primary mode (e.g., at 90-270 MHz) the LPA antenna will also beam downward, with an even sharper main lobe. The associated antenna pattern at this mode is more complex, and several sidelobes and nulls exist within the field of view of the Earth.

The FORTE RF payload relevant to the work presented in this paper includes a pair of independent radio receivers that each has an analog bandwidth of 22 MHz. The receivers can be tuned anywhere from 20 to 300 MHz. The gain for each receiver can be independently selected with a combination of RF amplifiers and attenuators. Each receiver's output is sampled continuously by a 12 bit digitizer at 50 mega samples per second. The digitizers can be synchronized to two independent frequency synthesizers or to a single synthesizer. Each receiver can be connected to either of the two LPA antennas and can be tuned to any frequency band. For polarization measurements to be presented in this paper, the two receivers were connected to the two different LPA antennas and were tuned to the same frequency band. The corresponding digitizers operated synchronously.

For the polarization observation experiments the receivers were tuned to the frequency bands of either 26-48 MHz ("low band") or 118-140 MHz ("high band"). In this paper, we will focus on the low-band observations.

### 3. Theory of Wave Polarization and Effects of Antenna Response

#### 3.1. Polarization Theory and Stokes Parameters

The electric field of a plane electromagnetic wave can be described, in general, as two linear components in the  $x$  and  $y$  directions in the plane normal to the wave propagation

$$\begin{aligned} E_x &= E_1 \sin(\omega t - \delta_x), \\ E_y &= E_2 \sin(\omega t - \delta_y). \end{aligned} \quad (1)$$

The wave can have linear, circular, or elliptical polarization, depending on the amplitudes  $E_1$  and  $E_2$  and the phase difference  $\delta_x - \delta_y$  between the two components. In general, a plane wave can be considered as elliptically polarized. Figure 1 shows the geometry for a right elliptical polarization in that the electric vector ( $\mathbf{E}$ ) rotates clockwise as the wave approaches the observer. The state of polarization for a completely polarized plane wave can be described by the tilt of the ellipse, the ratio of the minor to the major axes, and the sense of the rotation. In Figure 1,  $\tau$  denotes the tilt relative to  $x$ , and  $\varepsilon$  denotes the axis ratio in terms of an open angle and the sense of rotation in terms of its sign, where  $\tau$  can vary from  $-90^\circ$  to  $+90^\circ$  and  $\varepsilon$  can vary from  $-45^\circ$  to  $+45^\circ$ . The polarization will become linear as  $\varepsilon$  approaches zero, and will become circular as  $\varepsilon$  approaches  $\pm 45^\circ$ .

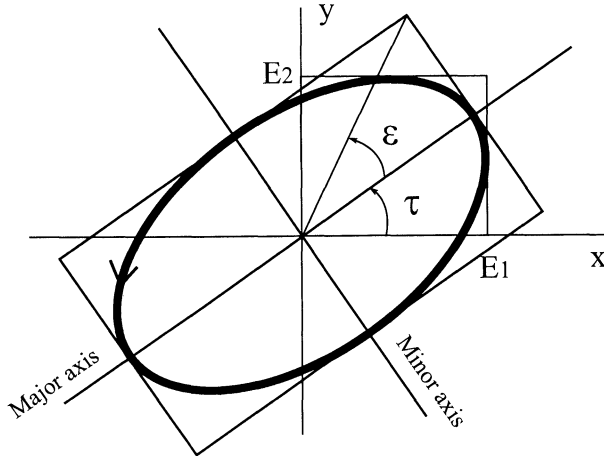


**Figure 1.** Geometry of polarization ellipse, illustrating relation of  $E_1$ ,  $E_2$ ,  $\tau$ , and  $\varepsilon$ .

To examine the state of polarization for a plane wave, Stokes parameters are introduced. The parameters are defined as [e.g., Kraus, 1986]

$$\begin{aligned} I &= E_1^2 + E_2^2 = P_0, \\ Q &= E_1^2 - E_2^2 = P_0 \cos 2\varepsilon \cos 2\tau, \\ U &= 2E_1 E_2 \cos(\delta_x - \delta_y) = P_0 \cos 2\varepsilon \sin 2\tau, \\ V &= 2E_1 E_2 \sin(\delta_x - \delta_y) = P_0 \sin 2\varepsilon. \end{aligned} \quad (2)$$

These equations describe a purely polarized wave with a total power of  $P_0$ . The four Stokes parameters are not entirely independent since they depend only on three variables ( $E_1$ ,  $E_2$  and  $\delta_x - \delta_y$ , or  $P_0$ ,  $\tau$ , and  $\varepsilon$ ), and they satisfy the relation

$$I^2 = Q^2 + U^2 + V^2. \quad (3)$$

In reality, a wave is more likely partially polarized so that  $E_1$ ,  $E_2$ , and  $\delta_x - \delta_y$  will change randomly with time rather than be constants. In this case, the measurable Stokes parameters will be expressed as

$$\begin{aligned} I &= \langle E_1^2 \rangle + \langle E_2^2 \rangle = P_0, \\ Q &= \langle E_1^2 \rangle - \langle E_2^2 \rangle = P_0 \langle \cos 2\varepsilon \cos 2\tau \rangle, \\ U &= 2\langle E_1 E_2 \cos(\delta_x - \delta_y) \rangle = P_0 \langle \cos 2\varepsilon \sin 2\tau \rangle, \\ V &= 2\langle E_1 E_2 \sin(\delta_x - \delta_y) \rangle = P_0 \langle \sin 2\varepsilon \rangle, \end{aligned} \quad (4)$$

where the brackets indicate the macroscopic time average.  $I$  and  $Q$  can be regarded as the sum and difference of two autocorrelation functions of  $E_1(t)$  and  $E_2(t)$ , while  $U$  and  $V$  can be regarded as the corresponding cross-correlation functions for the real and imaginary parts. In this case, (3) is no longer valid, but rather

$$I^2 \geq Q^2 + U^2 + V^2. \quad (5)$$

The ratio

$$d = \frac{\sqrt{Q^2 + U^2 + V^2}}{I}, \quad (6)$$

indicates the degree of polarization, which can vary in the range of 0-1 for completely unpolarized to completely polarized waves, respectively.

A partially polarized wave can be divided into two parts: (a) the completely unpolarized part and (b) the

completely polarized part. After normalizing (4) by the total power  $P_0$  the Stokes parameters can be rewritten as

$$S[s_i] = P_0 \begin{bmatrix} s_0 \\ s_1 \\ s_2 \\ s_3 \end{bmatrix} = P_0 \begin{bmatrix} 1-d \\ 0 \\ 0 \\ 0 \end{bmatrix} + P_0 \begin{bmatrix} d \\ d \cos 2\varepsilon \cos 2\tau \\ d \cos 2\varepsilon \sin 2\tau \\ d \sin 2\varepsilon \end{bmatrix}. \quad (7)$$

The first term at the right-hand side of the equation gives the unpolarized power, and the second term gives the completely polarized power. The parameters  $\tau$  and  $\varepsilon$  refer to the completely polarized part of the wave.

### 3.2. Effects of Antenna Pattern on Polarization Measurements

As described in section 3.1, with orthogonally oriented, linearly polarized receiving antennas, the polarization state of a plane wave can be completely observed. In the case that the wave front is parallel to the plane of the antennas, or with ideal isotropic antennas, one can promptly apply (4), (6) and (7) to determine  $P_0$ ,  $d$ ,  $\tau$ , and  $\varepsilon$ . In practice, as with the FORTE measurements, neither condition may be valid. In the following, we will lay out the theoretical basis for a general situation regarding both the effects of antenna beam pattern and the wave normal direction.

Figure 2 shows the framework for two linear polarization antennas and an arriving radio wave. The two antennas are in the directions of  $x$  and  $y$ , and the wave approaches from a direction defined by an azimuthal angle  $\varphi$  and a zenithal angle  $\theta$ . For the FORTE experiment the antenna in the  $x$  direction aligns with the satellite's ram direction, and the  $z$  direction coincides with the satellite's nadir. The incoming wave is assumed elliptically polarized. Prior to arrival at the antennas, the wave can be expressed in the same way as in (1), except in the coordinates of  $(\varphi, \theta, r)$ :

$$\begin{aligned} E_\varphi &= E_{\varphi_0} \sin(\omega t - \delta_\varphi), \\ E_\theta &= E_{\theta_0} \sin(\omega t - \delta_\theta). \end{aligned} \quad (8)$$

If both the antennas have isotropic patterns and unity gains, through geometrical transformations, the electric field detected by the antennas will be

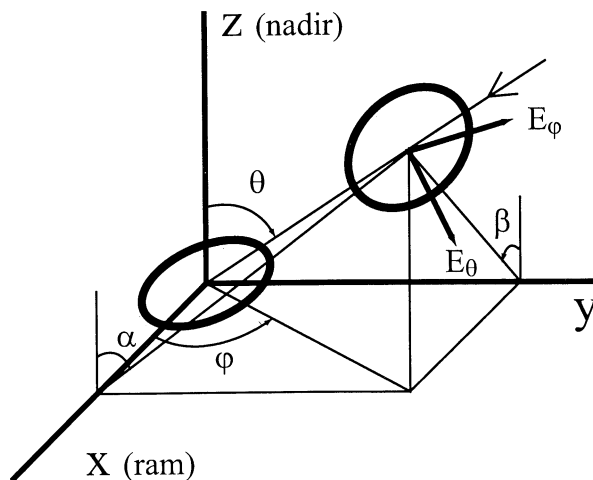


**Figure 2.** Illustration for an elliptically polarized wave approaching a cross-dipole antenna. The dipoles are along the  $x$  and  $y$  axes. Here,  $\varphi$  and  $\theta$  define the wave arrival direction. The ellipse on the  $x$ - $y$  plane is the antenna-detected ellipse of the original ellipse. For the FORTE satellite, positive  $x$  is aligned with the ram direction, and  $z$  is in the nadir direction.

$$\begin{aligned} E_x &= \frac{1}{\sqrt{1 - \sin^2 \theta \cos^2 \varphi}} (E_\theta \cos \theta \cos \varphi - E_\varphi \sin \varphi), \\ E_y &= \frac{1}{\sqrt{1 - \sin^2 \theta \sin^2 \varphi}} (E_\theta \cos \theta \sin \varphi + E_\varphi \cos \varphi), \end{aligned} \quad (9)$$

respectively.  $E_x$  is the projection of  $E_\theta$  and  $E_\varphi$  on the plane formed by the wave normal  $r$  and the  $x$  axis, with  $E_x$  perpendicular to  $r$ .  $E_y$  is the corresponding projection on the plane formed by  $r$  and the  $y$  axis. A practical antenna will not have an isotropic response. The response beam pattern (or directivity) can be expressed in the antenna's E plane and H plane separately with the overall beam pattern being approximated by the product of the two. As depicted in Figure 2, for the antenna along the  $x$  axis, its E plane pattern can be expressed as  $g_E(\beta)$  and its H plane pattern can be expressed as  $g_H(\alpha)$ , where

$$\begin{aligned} \tan \alpha &= \tan \theta \sin \varphi, \\ \tan \beta &= \tan \theta \cos \varphi. \end{aligned} \quad (10)$$

Here,  $\alpha$  and  $\beta$  are angles away from the broadside directions of the  $y$  and  $x$  antennas, respectively. Similarly, for an identical antenna along the  $y$  axis, its patterns are  $g_E(\alpha)$  and  $g_H(\beta)$ . Applying the antenna

patterns to (9) we have

$$\begin{aligned} E_x &= \frac{g_E(\beta)g_H(\alpha)}{\sqrt{1 - \sin^2 \theta \cos^2 \varphi}} (E_\theta \cos \theta \cos \varphi - E_\varphi \sin \varphi), \\ E_y &= \frac{g_E(\alpha)g_H(\beta)}{\sqrt{1 - \sin^2 \theta \sin^2 \varphi}} (E_\theta \cos \theta \sin \varphi + E_\varphi \cos \varphi). \end{aligned} \quad (11)$$

For an approaching wave which is originally elliptically polarized in the  $(\varphi, \theta, r)$  coordinates, (11) indicates that the corresponding signals detected by the antennas ( $E_x, E_y$ ) may not, in general, represent exactly an ellipse, but rather describe a wave with a distorted, quasi-elliptical polarization. In the special case that the approaching wave is circularly polarized, for instance,

$$\begin{aligned} E_\varphi &= \sin \omega t, \\ E_\theta &= \cos \omega t, \end{aligned} \quad (12)$$

we can come up with an analytical expression for the antenna-received signal. By substituting (12) into (11) we have

$$\begin{aligned} E_x &= g_E(\beta)g_H(\alpha) \sin(\omega t - \Delta_x + \pi), \\ E_y &= g_E(\alpha)g_H(\beta) \sin(\omega t + \Delta_y), \end{aligned} \quad (13)$$

where

$$\begin{aligned} \tan \Delta_x &= \frac{\cos \theta \cos \varphi}{\sin \varphi}, \\ \tan \Delta_y &= \frac{\cos \theta \sin \varphi}{\cos \varphi}. \end{aligned} \quad (14)$$

It is clear that (13) describes, in general, an elliptically polarized wave in the antenna plane. It becomes a circular polarization only if the wave approaches from the  $z$  direction, or the nadir direction for the FORTE satellite.

#### 4. Data Analysis and Results

Having presented a model, we now present the observations and data analysis in this section. We will focus on the observations of LAPP experiments and will present a case study for VHF lightning emissions. The LAPP was designed to produce high-power impulsive signals in the VHF part of the radio spectrum. The pulse width is typically 0.1  $\mu$ s or less. The impulsive signals are transmitted through a

broadband bowtie antenna so that the signals are approximately linearly polarized over a broad VHF range. The bowtie antenna is in turn located at the feed point of a 14-m-diameter parabolic dish, which is pointed to the satellite each time a signal is transmitted.

##### 4.1. Observations of Separate Ordinary and Extraordinary Modes

The combination of the Earth's ionospheric plasma and magnetic field acts as a birefringent medium for a radio signal and will split a linearly polarized radio signal into the ordinary and extraordinary modes [Budden, 1985]. At VHF the two modes should be nearly circularly polarized with opposite sense of rotation, if the wave normal  $\mathbf{k}$  is not nearly perpendicular to the direction of the magnetic field  $\mathbf{B}$ . If the collision and plasma frequencies of the ionosphere are much less than the radio frequency, which is true for the studies presented in this paper, the ratio of minor over major axes (Figure 1) for each mode can be approximated as

$$\tan|\varepsilon| = \frac{1}{2 \cos \gamma} \left[ \sqrt{\left(\frac{f_c}{f}\right)^2 \sin^4 \gamma + 4 \cos^2 \gamma} - \frac{f_c}{f} \sin^2 \gamma \right]. \quad (15)$$

Here,  $f$  is radio the frequency;  $f_c \equiv eB/2\pi m_e$ , the electron cyclotron frequency ( $B$  is the magnitude of the magnetic field vector  $\mathbf{B}$ ); and  $\gamma$  is the angle between  $\mathbf{k}$  and  $\mathbf{B}$ . The axis ratio will be 1 ( $\varepsilon = \pm 45^\circ$ ) if  $\gamma$  equals 0.

The impulsive nature of the LAPP signals and the difference of the group velocities for the two modes allow a detectable temporal separation (or "splitting") between the modes at the low end of VHF, as the signals travel from the Earth to FORTE [Massey *et al.*, 1998; Jacobson and Shao, 2001]. For cases in which the angle between  $\mathbf{k}$  and  $\mathbf{B}$  is not very close to a right angle, at VHF the group delays can be approximated as [Massey *et al.*, 1998]

$$t_g = \frac{R}{c} + \frac{a \text{ TEC}}{(f \pm f_c \cos \gamma)^2}, \quad (16)$$

where  $R$  is the distance between the LAPP and the FORTE,  $c$  is the speed of light,  $a$  is  $1.34 \times 10^{-7}$  when all quantities are expressed in mks units, and TEC is

the total electron content integrated along the line between LAPP and FORTE. The plus sign is for the ordinary mode, and the negative sign is for the extraordinary mode.

Plate 1 shows an observation for a single LAPP pulse. The experiment was conducted on June 5, 1998, at 1553:00 UT, when the satellite was at 31.67°N and 111.86°W. LAPP was, in turn, at 22.5° azimuth and 38.6° nadir as viewed by the satellite. The FORTE receivers were tuned to the 26-48 MHz band. For the analysis shown in Plate 1 we have not yet accounted for the effect of the antenna patterns but rather computed the state of polarization directly from the digitized records. The pattern effect will be examined later in detail with sequences of LAPP pulses.

Plate 1a shows the spectrogram for the total received power in decibel scale (as indicated by the colors) by the pair of antenna-receiver channels. For each channel the spectrogram is computed by taking Hanning-windowed Fourier transforms of 128 points and then "sliding" the window along the time axis by 2 points and repeating the process. The total power is then computed by adding the power values from the two channels, i.e.,  $E_1^2 + E_2^2$ . The magnetoionic splitting is clear from Plate 1a. The earlier pulse is associated with the ordinary mode, and the later is associated with the extraordinary mode (equation (16)). The overall dispersion for both the pulses is caused by the first-order ionospheric effect (the group delay varies as  $f^{-2}$ ).

Plate 1b shows the spectrogram for the degree of polarization  $d$ , as defined in (6). To compute  $d$ , the time-averaged  $I$ ,  $Q$ ,  $U$ , and  $V$  (equation (4)) are computed for each frequency component after the same "sliding" Fourier transforms as for the power spectrogram (Plate 1a). A Fourier transform of a time series will give both the amplitude and the phase of the transform, so that  $E_1$ ,  $E_2$  and  $\delta_x - \delta_y$  can be obtained for each of the associated frequency components. The time-averaging window is configured to include 100 sequential Fourier transforms along the time axis at 26 MHz and 60 at 51 MHz, which reflect actual time intervals of 4 and 2.4  $\mu$ s, respectively. Averaging windows for frequencies between 26 and 51 MHz decrease proportionally in width as frequency increases. This type of window size arrangement allows us to sharpen the time resolution as frequency increases, so as to accommodate the lesser temporal splitting at higher frequencies. The splitting between the two modes

varies as  $f^{-3}$ , as can be derived from (16). Each averaging window is also tapered with an appropriate Hanning window in order to reduce the sidelobe effects. As shown in Plate 1b, in which the colors indicate the degree of polarization from 0 to 1, both modes are highly polarized, as expected from the linear polarization of the LAPP pulse.

It needs to be pointed out that the relatively high degree of polarization computed in the absence of any signal is due to the finite sizes of the Fourier window and the subsequent time-averaging window applied to the data analysis. The degree of polarization is essentially a measure of correlation between the two signals detected by the two orthogonal antennas. For purely random, unpolarized background noise the degree of polarization is expected to be zero. With a finite number of data samples (e.g., finite averaging window) the correlation between two random, independent sequences will be artificially elevated. The selection of the Fourier and averaging window sizes in this study is to allow a balanced temporal and frequency resolution. Nevertheless, since the LAPP pulses are known to be highly polarized, the measure of the degree of polarization is not very critical in this paper.

Plate 1c shows the observations for the tilt of the polarization ellipse  $\tau$ , in that the colors indicate the tilt angles in the range of  $-90^\circ$  to  $+90^\circ$ , relative to the ram direction (positive  $x$  in Figure 2) of the satellite. In Plate 1c, as well as in Plate 1d, results are shown only where the associated power intensity greater than  $-90$  dB (Plate 1a). At places where the power is less, red color is used. The tilt angle is computed by using  $s_1$ ,  $s_2$ , and  $d$  in (7) with the same Fourier transforms and time averaging as for  $d$  (Plate 1b). We see that  $\tau$  is somewhere about  $-70^\circ$  for both the modes across the frequency band. Noticing that the LAPP was at 22.5° azimuth as viewed from the satellite,  $\tau$  is determined by a direction orthogonal to the wave normal, which would be  $-67.5^\circ$ . This should be expected since a circular polarization will be compressed into an elliptical polarization with the major axis orthogonal to the wave propagation, as it arrives at the FORTE antennas from directions (38.6° in this case) other than the nadir.

Plate 1d shows the sense of the rotation and the axis ratio  $\varepsilon$  for the polarization ellipses for the two modes, in the same format as for Plate 1c. It is computed the same way as for  $\tau$ , but by using  $s_1$  and  $d$  in (7). The colors are used to show  $\varepsilon$  in the range of  $-45^\circ$  to  $+45^\circ$ .

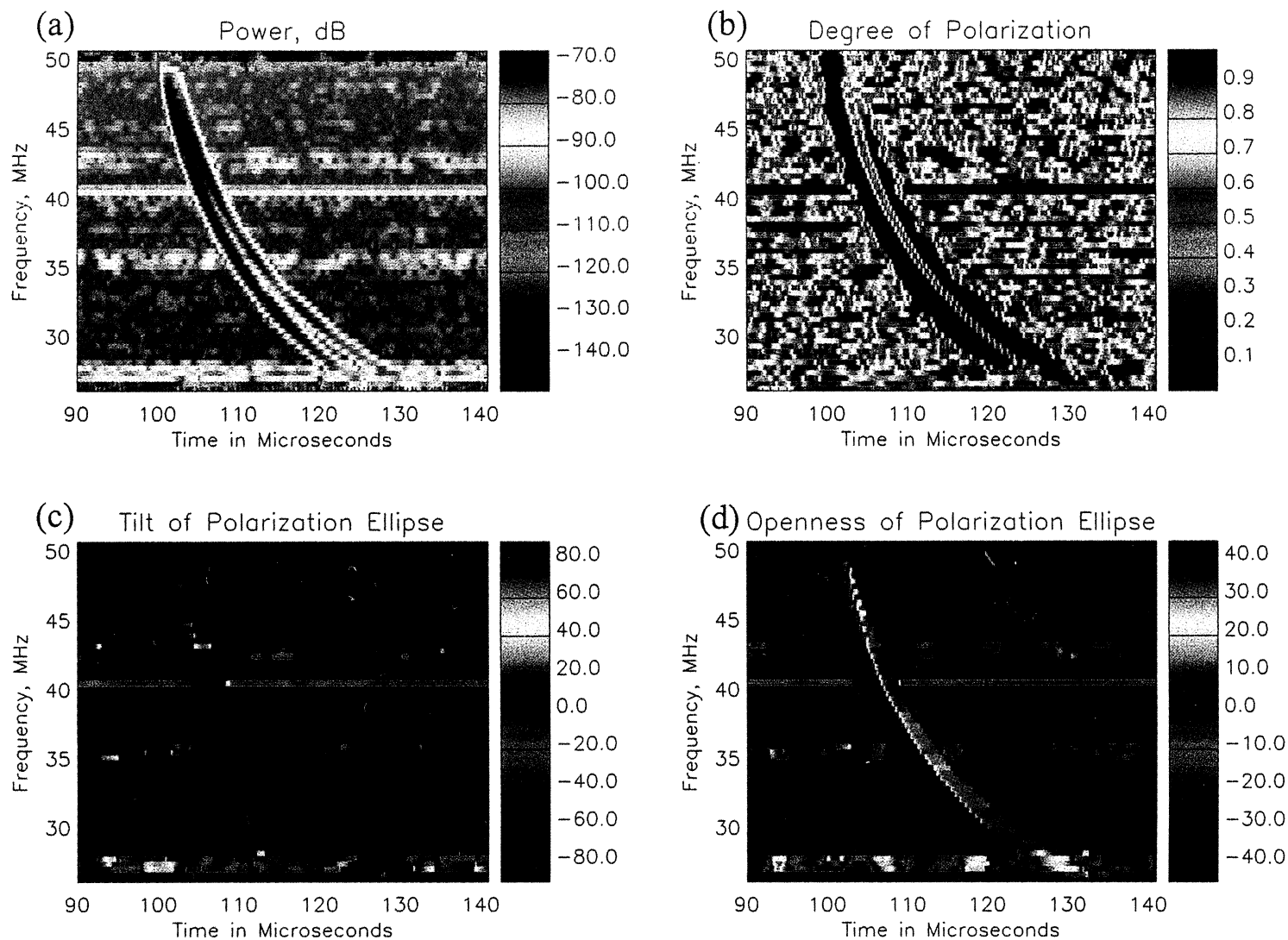


**Plate 1.** Polarization observations for a LAPP pulse obtained on June 5, 1998 at 1553:00 UT. (a) Spectrogram of the total power from both the LPA antennas. (b) Degree of polarization  $d$ , color-coded from 0 to 1. (c) Tilt angle of the polarization ellipse  $\tau$ , color-coded from  $-90^\circ$  to  $+90^\circ$ . (d) Openness of the polarization ellipse and the sense of the rotation  $\varepsilon$ , color-coded from  $-45^\circ$  to  $+45^\circ$ .

As stated before, for circular and linear polarizations,  $\varepsilon$  equals  $\pm 45^\circ$  and  $0^\circ$ , respectively; for elliptical polarization,  $\varepsilon$  has a value between the two. Plate 1d shows that  $\varepsilon$  is about  $-30^\circ$  for the ordinary mode and about  $+30^\circ$  for the extraordinary mode. The magnitudes of  $\varepsilon$  indicate that the two modes detected by FORTE are elliptically polarized with about the same axis ratio. As discussed above for  $\tau$ , the presumably original circular polarization for each mode is compressed into elliptical polarization onto the antenna plane since the wave arrives from an angle  $38.6^\circ$  away from the nadir. The negative sign is for anticlockwise rotation, and the positive sign is for clockwise rotation, as expected by looking downward at the two modes over the Earth's Northern Hemisphere.

Having presented the case study above, we have described the methodology implemented for the data analysis. We are now ready to investigate a collection of similar LAPP observations. In June of 1998 we conducted 125 low-band FORTE-LAPP experiments. Among these, 81 were measured coherently between the two antennas and the corresponding receivers and can be studied for polarization properties.

We first dechirp the time series data coherently (i.e., preserving phase) for each of the two sets of records, so that the LAPP pulse at different frequency components will appear to arrive at the satellite at the

same time rather than with increasing delays as frequency decreases. The result of the dechirping is that the chirp-shaped feature presented in Plate 1 will be transformed to a near-vertical feature, as shown in Plate 2. The dechirping is done by finding a slant TEC value that optimally aligns the power spectrogram into a vertical feature according to the first-order ionospheric relation  $t \propto \text{TEC } f^{-2}$ . Such a dechirping process has been described in detail by *Jacobson et al*, [1999]. Apparently, with a significant mode splitting, such a dechirping will yield TEC estimates with considerable uncertainties, probably up to 10% for some of the LAPP observations presented in this paper. For instance, as shown in Plate 2, the TEC found through such an optimizing process serves to align vertically for the ordinary mode but not at the same time for the extraordinary mode. For the purpose of the polarization study we dechirp the data from one antenna first and find the best fit TEC and then dechirp the other antenna's data by using the same TEC.

After the dechirping, the data are processed the same way as for the above case study. We then determine an average value for each of the four parameters (as shown in Plate 1) within a 4 MHz subband centered at 34 MHz (as illustrated in Plate 2 for the power) for a given time and repeat the same process forward along the time axis. The subband is so

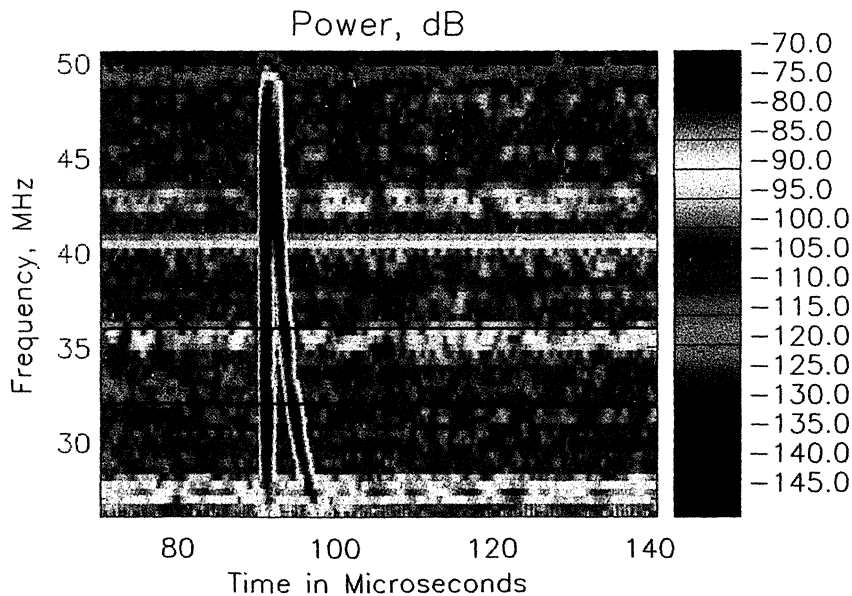


**Plate 2.** Same as Plate 1a, but after dechirping the data with an optimal TEC value.

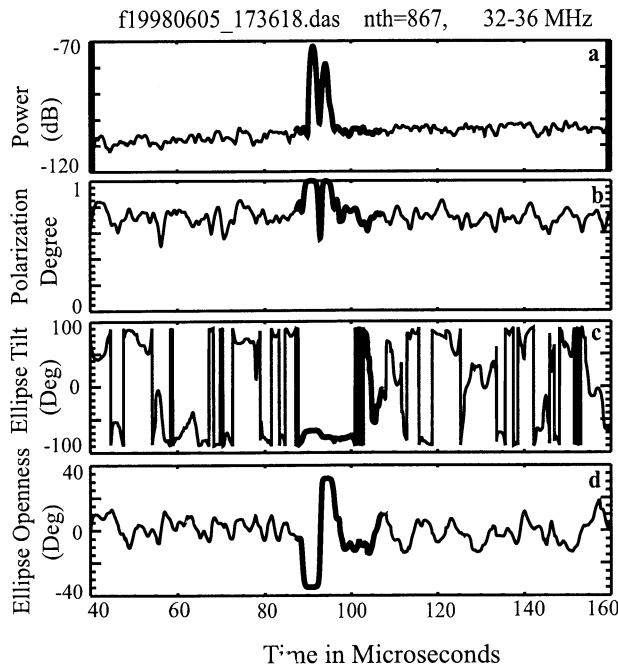


**Figure 3.** (a) Power, (b) degree of polarization  $d$ , (c) tilt angle of polarization ellipse  $\tau$ , and (d) openness of polarization ellipse  $\varepsilon$ , as averaged within 4 MHz centered at 34 MHz.

selected to avoid possible interfering carrier signals (as at about 27 and 40 MHz), as well as to assure a detectable temporal separation between the two modes. The mean values are then regarded as representative values for the four associated parameters. An example for such data processing is shown in Figure 3. The original data are the same as for the above case study (Plate 1). Figure 3 shows the subband-averaged values for the power, degree of polarization, tilt angle, and openness of the ellipse, from the top plot to the bottom, respectively. The mode splitting is represented by the double peaks in Figures 3a and 3b, as well as in Figure 3d by the corresponding opposite values of  $\varepsilon$ . Same as illustrated in Plate 1, Figure 3 shows that the pulse is highly polarized with  $d=1$  for both of the modes,  $\varepsilon$  equal to about  $-30^\circ$  and  $+30^\circ$  for the ordinary and extraordinary modes, respectively, and  $\tau$  equal to about  $-70^\circ$  for the ordinary mode and slightly less for the extraordinary mode.

All 81 pulses are then dechirped and analyzed. For each pulse,  $\tau$  and  $\varepsilon$  are determined for each of the two modes. The polarization degree  $d$  is found to be

almost 1 for each pulse, as expected for LAPP. Results for  $\varepsilon$  will be discussed first, and together the antenna pattern effects on the observation of  $\varepsilon$  will be introduced and discussed.

Figure 4 shows  $\varepsilon$  as a function of the angle away from the satellite's nadir direction for the 81 LAPP pulses. The diamond and square symbols indicate  $\varepsilon$  for the ordinary and extraordinary modes, respectively, for each corresponding pulse. All the ordinary modes rotate anticlockwise ( $\varepsilon < 0$ ), whereas all the extraordinary modes rotate clockwise ( $\varepsilon > 0$ ), as expected for viewing the radio signal over the Earth's Northern Hemisphere. Close to the nadir direction, at which LAPP is nearly underneath the satellite, both modes are observed nearly circularly polarized with  $\varepsilon$  close to  $\pm 45^\circ$ . As the nadir angle increases, both modes converge almost symmetrically toward linear polarization, as  $|\varepsilon|$  moves toward 0. This near-mirror-image appearance between the two modes shows that the two modes are identical in terms of polarization with, of course, opposite sense of rotation. The observations stop at a nadir angle of  $\sim 63^\circ$ , the Earth's limb as seen by the satellite. This general feature of the change of  $\varepsilon$  is caused by the antenna patterns, as we discuss now.

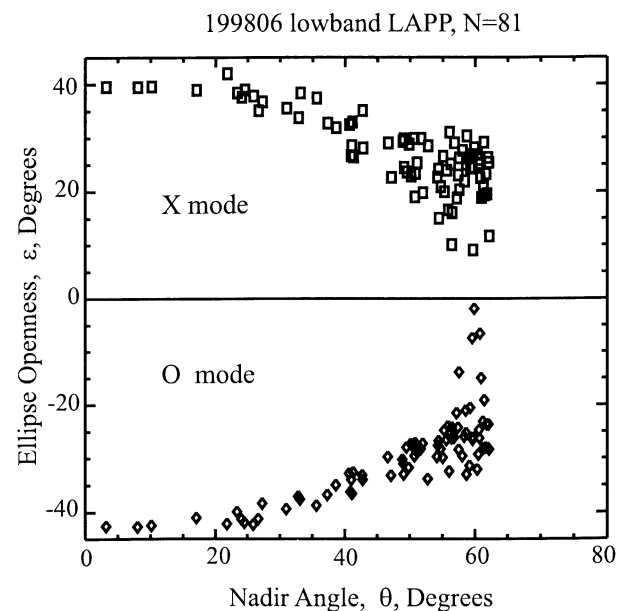


**Figure 4.** Openness of the polarization ellipse as a function of the nadir angle. The diamond symbols are for the ordinary modes, and squares are for the extraordinary modes.

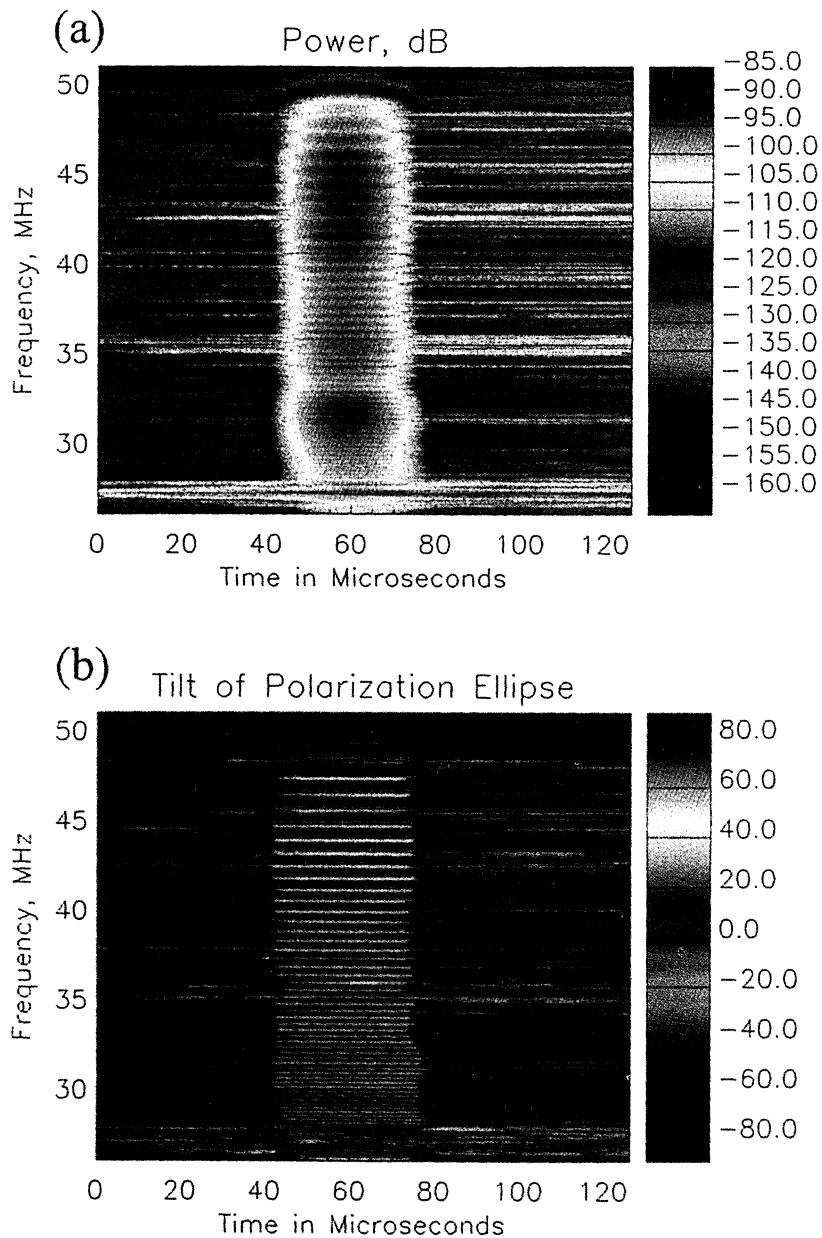


**Plate 3.** Same LAPP pulse as shown in Plate 1. The two modes are mixed together by using a wider Fourier window to show the Faraday rotations. Signal is dechirped prior to the polarization analysis.

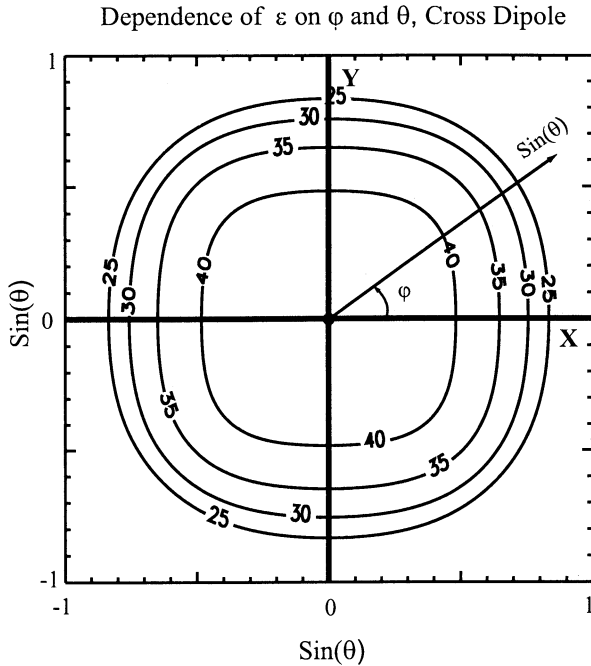


**Figure 5.** Cross-dipole detected openness of polarization ellipse  $\epsilon$  for originally circularly polarized signal arriving from  $(\varphi, \theta)$ . Here,  $\epsilon$  is shown as contours in the plane of the dipoles.

Equation (13) describes responses of orthogonal linear polarized antennas for an approaching plane wave with circular polarization. Substituting this equation into (2), the polarization state that accounts for the antenna responses can be resolved. As stated in section 2, the FORTE antenna is expected to have a moderate gain in its forward direction. However, since the results presented in Figure 4 are for the frequencies around 34 MHz, only the longest element in each LPA will participate as an active receiving element, which should then perform as a dipole antenna. Without losing generality we will approximate an antenna pattern with the form of

$$g(\alpha) = \frac{\sin(2\pi\alpha/BW)}{(2\pi\alpha/BW)}, \quad (17)$$

for both that in  $E$  and  $H$  planes, where  $BW$  is the beam width between the first nulls. A  $\lambda/2$  dipole antenna has a  $180^\circ$  beam width in its  $E$  plane ( $BW = \pi$ ) and has a uniform response, or an infinite beam width, in its  $H$  plane ( $BW = \infty$ ).

Figure 5 shows the expected  $\epsilon$  due to applying (17). The computed  $\epsilon$  is shown as contours on the plane of

the cross-dipole antenna, in which the radial distance between the origin and a point reflects  $\sin(\theta)$ , where  $\theta$  is the zenith (or nadir) angle (Figure 2). It is clear that  $\epsilon$ , as shown by the labeled contours, is dependent on both the nadir and azimuthal angles. Here,  $|\epsilon|$  is expected to be  $45^\circ$  at the center and is to become smaller as  $\theta$  increases. It is also clear that a wave arriving from an azimuth between the two dipoles appears more circular than one arriving along one of the antennas.

Figure 6 plots the measured  $\epsilon$  for the ordinary mode (as in Figure 4) against the computed  $\epsilon$  from the antenna model. They have a general agreement, indicating that the polarization before projection is circular in general. The discrepancy between the two analyses increases as  $|\epsilon|$  becomes smaller, and there are four points that appear much more toward linear polarization from the measurement than from the prediction. Comparing Figures 6 and 4, the larger discrepancies occur when the corresponding nadir angles are near  $50^\circ$  or beyond. Several different ionospheric effects are accounted for the increasing discrepancies. First, as nadir angle increases, the actual ray path of the wave differs more as compared to the line of sight between the LAPP and the satellite. This ray-bending effect of the ionosphere can introduce a few degrees of error for the actual arrival direction (at frequencies near 34 MHz) if the nadir angle is  $50^\circ$  or greater. The other effect is entirely

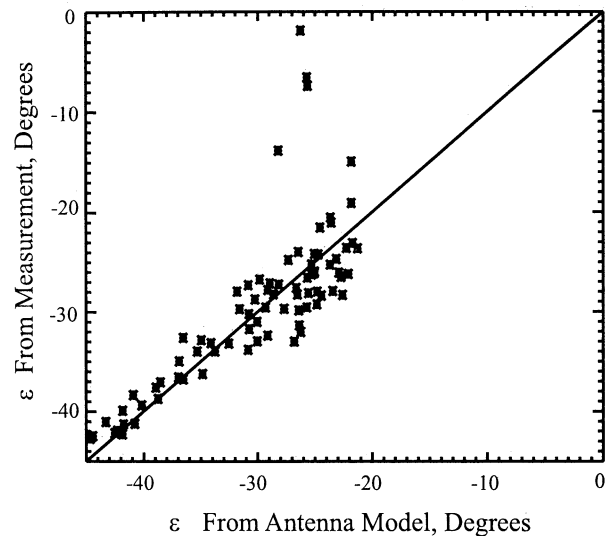


**Figure 6.** Comparison between the modeled and the measured  $\epsilon$ .

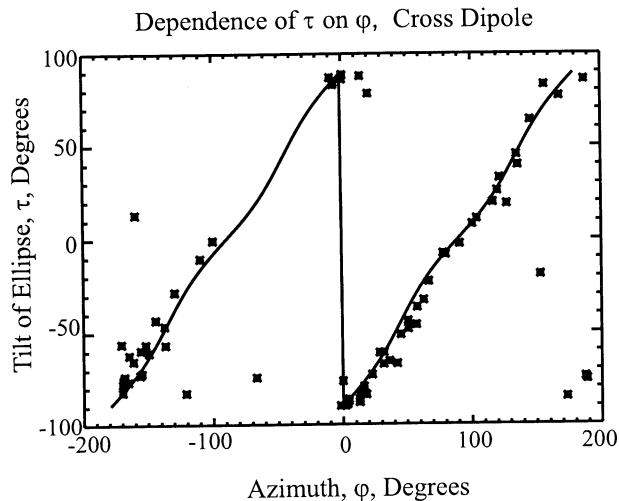


**Figure 7.** Comparison between the modeled (solid line) and the measured  $\tau$ . Here,  $\tau$  repeats two cycles of  $-90^\circ$  to  $+90^\circ$  as  $\phi$  varies from  $-180^\circ$  to  $+180^\circ$ .

related to the Earth's magnetic field. At low VHF it is usually valid to assume that each of the split modes be circularly polarized. However, as the vectors of the wave normal  $\mathbf{k}$  and the magnetic field  $\mathbf{B}$  are nearly perpendicular to each other, each mode becomes elliptically polarized. For example, if FORTE is at ( $54.1^\circ\text{N}$ ,  $113.1^\circ\text{W}$ ), the angle between  $\mathbf{k}$  and  $\mathbf{B}$  will be  $87^\circ$ , and the original axis ratio for each mode, prior to being detected by the satellite, is  $\sim 0.72$ , or  $35.8^\circ$  in terms of  $\varepsilon$ . This is the case for one of the four data points that differ significantly from the model. The geomagnetic field is computed at the point of the satellite, according to the International Geomagnetic Reference Field (IGRF) model [Langel, 1992]. An ellipse detected by FORTE could be further elongated or shortened, depending on the direction of the arrival of the wave and the direction of the magnetic field. In this case, the measured  $\varepsilon$  will diverge from what the model predicted for an upcoming circular polarization. Indeed, for the four points that are far different from the model (Figure 6) we found that the corresponding angles between  $\mathbf{k}$  and  $\mathbf{B}$  are in the range of  $84^\circ$  to  $87^\circ$  and FORTE was far north or northwest of the LAPP.

We now present the observations for the tilt of the polarization ellipse  $\tau$  and compare the results with the cross-dipole antenna model. Figure 7 shows the measured and the model-predicted (solid line)  $\tau$  as a function of the azimuthal angle  $\phi$ , where  $\phi$  is counted from the ram direction of the satellite, or the direction

of antenna  $x$  in Figure 2, which by design is aligned in the direction of satellite trajectory. The tilt angle varies from  $-90^\circ$  to  $+90^\circ$  and will have the same value as the wave arrives from two opposite directions. It is clear that the orientation of the ellipse  $\tau$  detected by the satellite is approximately perpendicular to the arrival direction  $\phi$  of the wave. As in Figure 6, there are also four data points that appear to be far away from the model. These discrepancies are caused by the same effect described earlier.

#### 4.2. Observations of Faraday Rotations

In the analysis in section 4.1 we have chosen a relatively narrow Fourier window (128 points) so that the two modes can be examined separately. If the two modes are coupled with each other, the resultant wave will be nearly linearly polarized with the plane of polarization rotating continuously as it propagates through the Earth's ionospheric plasma and magnetic field. This phenomenon is called Faraday rotation [Davies, 1990]. The total amount of rotation for a transionospheric VHF signal can be approximated as, in units of radians,

$$\Psi = 2.366 \times 10^4 \frac{B \cos \gamma}{f^2} \text{TEC}. \quad (18)$$

Here,  $B$  is the magnetic field at an effective ionospheric height, usually  $\sim 400$  km above the Earth surface. Faraday rotation has been used previously by many researchers to study the TEC and its temporal variations [Davies, 1980]. Early transionospheric studies have usually implemented a single frequency or a few discrete narrowband satellite beacons to monitor the total rotation of the E vector. To the authors' knowledge, no observation of Faraday rotation has been reported for broadband VHF signals. With a broadband VHF signal,  $\Psi$  will change continuously within the frequency band; therefore no rotation ambiguity in terms of the total number of cycles will be involved, as typically faced by a single VHF frequency measurement. The relative rotation between two different frequencies can be measured, and the TEC can be determined. Many other techniques, based on either satellite beacons (e.g., the Global Positioning System, see Ho *et al.* [1997]) or ground radars [e.g., see Farley, 1991], have been developed to monitor the TEC and the electron density profile within the Earth's ionosphere. Experiments with transionospheric broadband VHF Faraday

rotation, as presented in this paper, provide an alternate means for TEC observation.

The same set of LAPP data will be analyzed for the Faraday rotation. To do this, we choose a much wider Fourier window to intentionally mix the two modes together. Plate 3 illustrates such an analysis for the same LAPP pulse as shown in Plate 1. The signals from the two antennas are first coherently dechirped, as described in section 4.1, so the peak powers at different frequencies appear to arrive at the satellite at the same instant. We then process the data in the same way as that for Plate 1, but with a Fourier window of 2048 points (instead of 128 points). The corresponding time-averaging window is also increased from 4 to 32  $\mu$ s for 26 MHz. The power spectrogram (Plate 3a) is now widened in the time axis and no longer shows the mode splitting. The tilt angle of the E vector  $\tau$  (Plate 3b) can be seen going

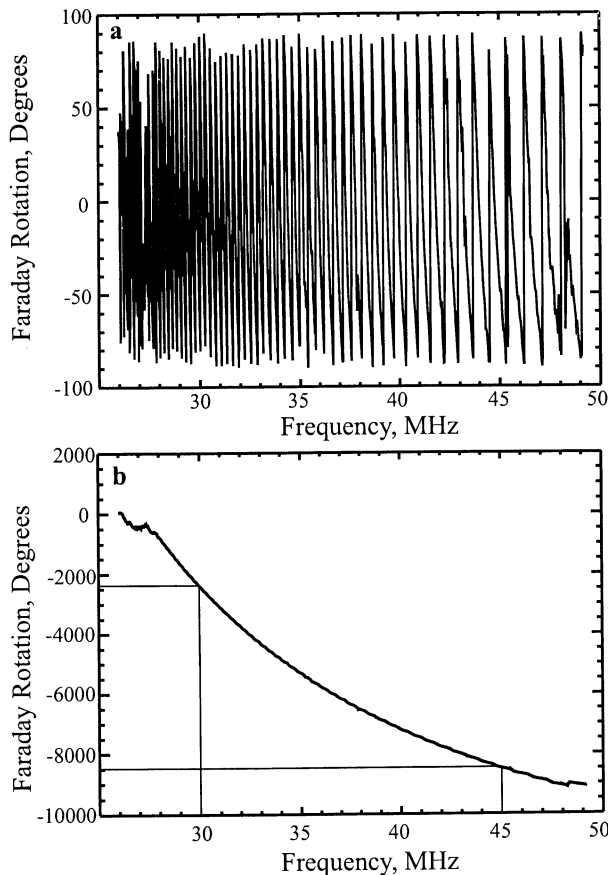


**Figure 8.** Faraday rotation as a function of frequency. (a) Crosscut through frequency at time equals 60  $\mu$ s of Plate 2b. (b) Unwrapped from Figure 8a.

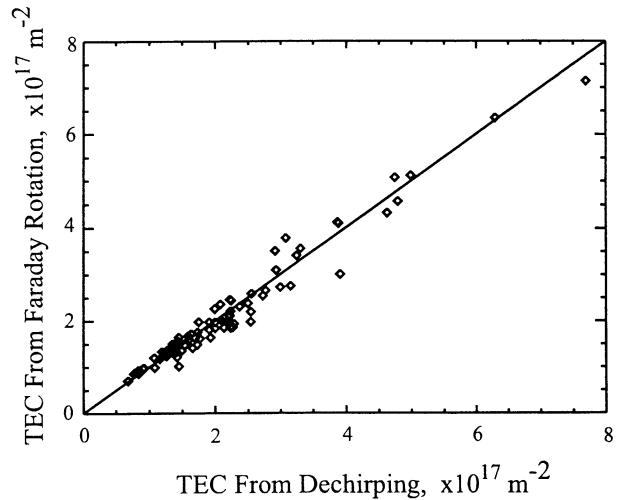


**Figure 9.** TEC resolved from Faraday rotation against TEC from dechirping of the signal.

through many 180° cycles as frequency varies from 26 to 48 MHz. The general trend of slowing of the rotation with increasing frequency is also clearly shown in Plate 3b, as will be expected from (18). In addition to intentionally mixing the two modes the wider Fourier window also serves to increase the frequency resolution so that the Faraday rotation can be more accurately examined.

Figure 8a is a cross section of Plate 3b at 60  $\mu$ s, showing the Faraday rotation as a function of frequency. Figure 8b shows the same rotation result after unwrapping the repeated 180° cycles. It shows more clearly the  $f^{-2}$  dependence of the Faraday rotation. By selecting two frequencies and their corresponding Faraday rotation angles we can determine the slant TEC if  $B \cos(\gamma)$  is known, or vice versa, according to (18). For this LAPP pulse,  $\Psi$  is  $-2400^\circ$  and  $-8500^\circ$  at frequencies 30 and 45 MHz, respectively. Since the locations of the satellite and the LAPP are both known, we can estimate  $B \cos(\gamma)$  to a reasonable accuracy. From the IGRF model,  $B \cos(\gamma)$  equals  $3.749 \times 10^{-5} \text{ Wb m}^{-2}$ , by choosing 400 km above the Earth as the effective height of the ionosphere. From (18), we found that the slant TEC equals  $1.94 \times 10^{17} \text{ m}^{-2}$ . For comparison, the TEC computed from the dechirping of the signal is  $1.75 \times 10^{17} \text{ m}^{-2}$ .

In order to analyze the large number of pulses automatically, for each pulse we select the frequency-tilt-angle cross section (as shown in Figure 8a) at the

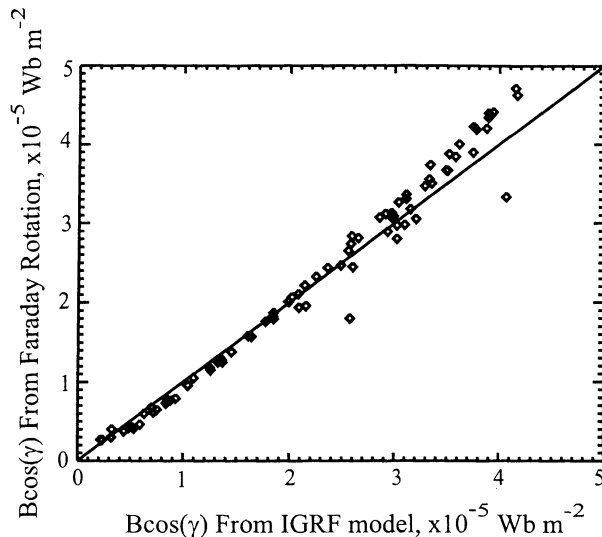


**Figure 10.** Longitudinal magnetic field  $B \cos(\gamma)$  computed from Faraday rotation compared to that from IGRF model.

time when the power peaks. The power is computed by averaging the vertical column for each given time in the two-dimensional time-frequency matrix. The rest of the analyses are the same as we just described for the above case study.

Figure 9 compares, for all 81 pulses, the TEC values computed from the Faraday rotations against the TEC values that resulted from the dechirping process. The former computation depends solely on the Earth's magnetic field, whereas the latter depends only on the relative group time delays at different frequencies. TEC values resolved from these two entirely independent means, however, agree with each other fairly well. It is not immediately clear what causes the residual scattering in the plot. TEC computed from the Faraday rotation could be affected by the bending of the ray path, so that the actual angle between  $\mathbf{k}$  and  $\mathbf{B}$  will differ from what the model indicates. On the other hand, TEC from the dechirping could be contaminated by the temporally split modes, as described in section 4.1 and shown in Plate 2, which can probably lead to up to 10% uncertainties for some of LAPP observations.

We can also compare the longitudinal magnetic field  $B \cos(\gamma)$  between the IGRF model and the Faraday rotation. To do this, TEC values from the dechirping will be used. It is clear that this comparison is not physically different from the TEC comparison we just described, but only provides a different point

of view for looking at the data. Figure 10 shows such a comparison. Besides the good agreement between the two, it is noticed that at higher  $B \cos(\gamma)$  the measured results are greater than the modeled results, whereas at lower  $B \cos(\gamma)$  the opposite tendency can be seen. The TECs obtained through the dechirping should not, in principle, correlate with the magnetic field and therefore would be less likely accounted for by this seemingly systematic discrepancy. Given the geolocation of the LAPP (35.87°N, 106°W),  $\mathbf{k}$  and  $\mathbf{B}$  will be parallel if FORTE is at ~32°N latitude while in the same meridian plane as the LAPP. If FORTE is south of 32°N, the bending of the actual ray path will favor a decrease of the angle between  $\mathbf{k}$  and  $\mathbf{B}$  compared to the angle between the line of sight and  $\mathbf{B}$  (the model). North of 32°N the actual angle will be greater than the modeled angle. This type of ray-bending effect, combined with the fact that  $\mathbf{k}$  and  $\mathbf{B}$  are closer to parallel in the south (therefore greater  $B \cos(\gamma)$ ) and closer to orthogonal in the north (lower  $B \cos(\gamma)$ ), is probably the reason for the discrepancies between the model and the measurement. For the case where FORTE is either east or west of LAPP the corresponding latitude at which  $\mathbf{k}$  and  $\mathbf{B}$  are parallel will be greater than 32°N.

#### 4.3. Observations of Lightning-Produced Signals: A Case Study

Since it was launched in August 1997, FORTE has recorded millions of VHF signals produced by lightning discharges. Many of the data were taken coherently by the two LPA antennas and are ready to be analyzed for polarization properties. In addition to the ionosphere studies the polarization investigations of VHF signals produced by lightning discharges will help us to understand the basic breakdown processes involved in the discharges. Polarization observations for lightning VHF signals have not been reported in the literature, simply because such observations are complicated to conduct on the ground. One would have to be very careful to sort out the effects of the conducting ground and the surrounding structures near the sensor over the measurement. Without these environmental complexities the FORTE satellite provides an ideal platform for the polarization observations. As a thorough study of lightning signals is beyond the scope of this paper, we present here only an example of the observations. A more complete study focusing on the lightning signals will be presented in a later paper.

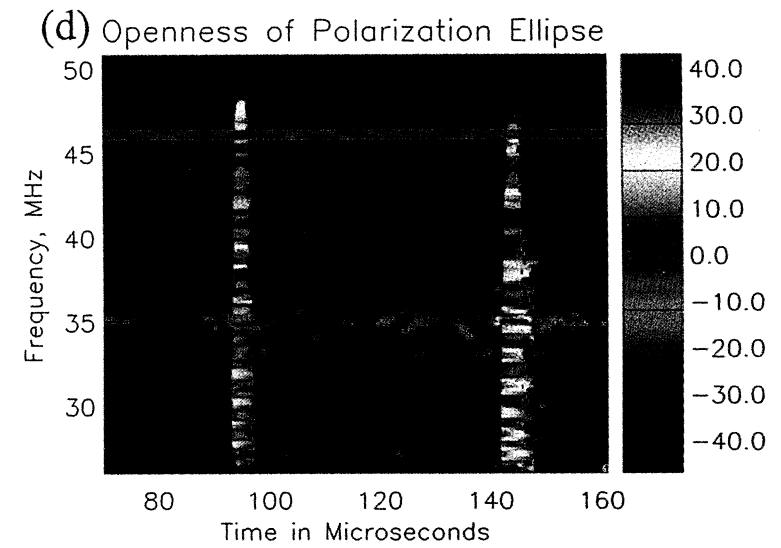
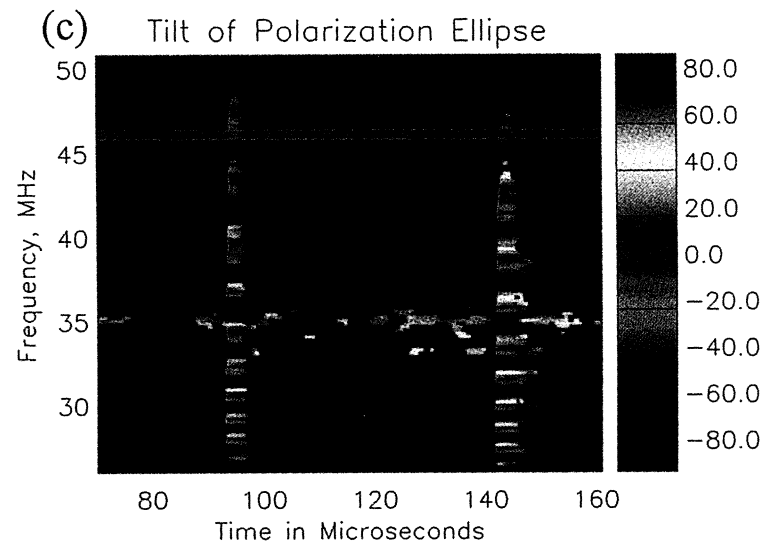
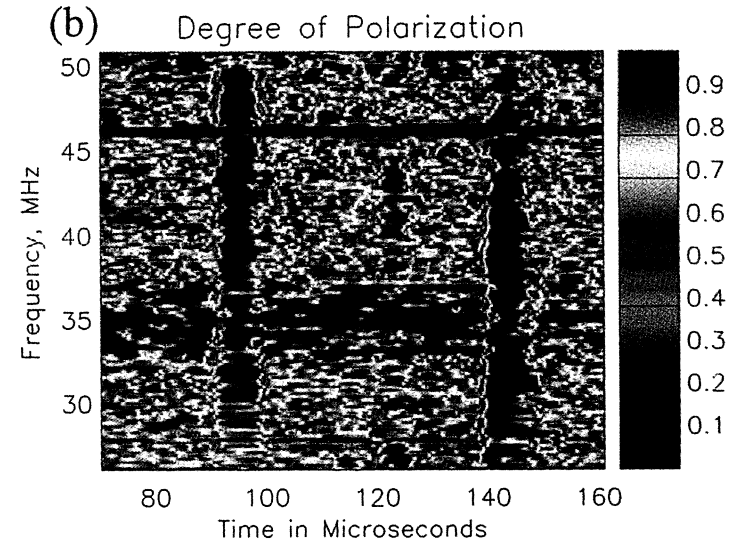
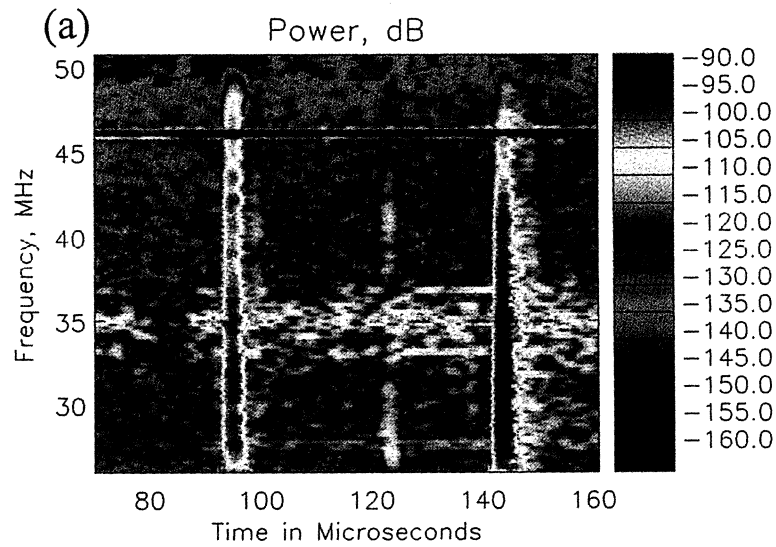


**Plate 4.** Polarization observations for a lightning-produced TIPP event. Results are shown in the same format as in Plate 1 except that the signal is dechirped first. There is no apparent mode splitting in this case, but Faraday rotation can be clearly seen.

Plate 4 shows polarization observations for a lightning-produced transionospheric pulse pair (TIPP) event [Holden *et al.*, 1995; Massey and Holden, 1995]. The first pulse of the pair propagates to the satellite directly from its source, while the second pulse is a replica of the first but travels to the satellite after being reflected from the surface of the Earth [Jacobson *et al.*, 1999]. This event was observed at 1729:11 UT on September 13, 1999, when the FORTE satellite was over the equator (2.78°S, 154.08°E). The data are analyzed and presented in the same way as done in Plate 1, except that the signals are dechirped first. The TEC obtained from the dechirping is  $0.795 \times 10^{17} \text{ m}^{-2}$ .

There is no clear mode splitting for each of the two TIPP pulses, because the TEC and/or  $B \cos(\gamma)$  are small (equation (16)). From the TEC value and the measurement of Faraday rotations (first pulse in Plate 4c) we found that  $B \cos(\gamma)$  equals  $1.47 \times 10^{-5} \text{ Wb m}^{-2}$ . Comparing this TEC value to that obtained from the LAPP pulses (Figure 9), it is indeed smaller than most of those. The value for  $B \cos(\gamma)$  for this event is also in the lower range of that obtained from the LAPP observations.

Plate 4b shows that both pulses are highly polarized, indicating that the associated breakdown processes are unique and highly organized. This finding is new since no polarization observations have been reported before for lightning VHF signals.

Plate 4c shows the Faraday rotations for the pair of pulses. The Earth-reflected pulse has about the same rotations as the original pulse, indicating that they traveled along about the same path through the Earth's ionosphere. The pulses are found to be mostly linearly polarized as shown by Plate 4d. It is not clear, though, what causes the variations of the  $\epsilon$  along the frequency. It is noticed that the  $\epsilon$  variation occurs concurrently with the rotation of  $\tau$ , appearing to suggest that the two modes were originally elliptically polarized prior to arrival to the satellite. For the purpose of comparison the carrier signal at ~42 MHz is detected purely linearly polarized.

## 5. Summary and Discussion

In this paper, we have presented polarization observations and analyses of broadband VHF signals detected by the FORTE satellite. The orthogonally oriented, linearly polarized FORTE LPA antennas, together with the corresponding phase-locked radio

receivers, allow us to investigate the complete polarization properties for a received signal. For each signal a complete set of Stokes parameters are computed in a two-dimensional time-frequency domain, which in turn can be further examined to obtain the degree of polarization, the tilt and the axis ratio of the polarization ellipse, and the sense of the E vector rotation.

With the impulsive nature of the LAPP transmitted pulses, polarization has been determined for each of the two temporally split ionospheric radio modes, the ordinary and extraordinary modes. Together with the considerations of the FORTE antenna pattern, each mode was determined to be nearly circularly polarized at the lower end of VHF, agreeing with the theoretical prediction. With the given response patterns of the FORTE antennas the original circular polarization will appear as an elliptical polarization. The tilt of the polarization ellipse, as referenced to the satellite's ram direction, has been analyzed and has shown good agreement with the antenna model. The analysis for the split modes was carried with a narrow Fourier window (128 points) in order to separate the modes in the time domain.

With the same set of data we have also studied the ionospheric Faraday rotation. For the purpose of this type of study we widened the Fourier window to 2048 points so that the two split modes were intentionally mixed together. The wider Fourier window also serves to increase the frequency resolution so that the Faraday rotation as a function of frequency can be more accurately determined. With the broadband signal the total cycles of Faraday rotations between a pair of frequencies can be accurately and unambiguously determined. With the known locations of the satellite and LAPP the slant TEC was computed for each of the LAPP pulses. The TEC obtained by this means agrees with the TEC that resulted from the dechirping of the signal. The two methods are independent of each other.

We also presented an observation for a lightning-produced TIPP event. This TIPP event is highly polarized, indicating that the associated breakdown processes are highly organized, rather than being a swarm of randomly oriented sparks. More observations of lightning RF emissions related to different types of discharges will be presented in a following paper.

Having summarized the two methods of data analysis, we note that an impulsive broadband VHF

source near the surface of the Earth, such as those produced by lightning discharges, could be located with the polarization observations. As from the observations of the separate modes, the tilt of the detected ellipse gives the azimuthal direction of the source with one ambiguity (Figure 7). The detected axis ratio describes a locus of points on the surface of the Earth with the center of the locus at the subsatellite point (Figure 4). From the observations of the Faraday rotation,  $B \cos(\gamma)$  can be measured (Figure 10), if the corresponding TEC is known. As described in section 4.1, TEC can be resolved by dechirping the broadband signal to best fit the  $f^{-2}$  dependence. TEC can also be resolved by examining the beating frequency between the two modes [Massey et al., 1998]. The measured  $B \cos(\gamma)$  then specifies another locus of the points on the Earth's surface. This locus will be different from the locus projected by the axis ratio, except at the North or South Poles. Comparing  $B \cos(\gamma)$  with the two possible locations, one could potentially find the actual location for the source. Instead of from Faraday rotation,  $B \cos(\gamma)$  can also be determined by the examination of the beating frequency between the two modes, as reported previously [Jacobson and Shao, 2001], which by itself can be used to locate a repeated radio source.

We noticed, though, for the data presented in this paper the dependence of the axis ratio on the nadir angle is rather insensitive, simply because the antennas have a rather flat beam at the frequencies studied. Further studies are needed for higher-frequency measurements to see if the sensitivity can be improved.

**Acknowledgments.** We thank Daniel Holden, Dave Smith, and Gary Stelzer for operation of the LAPP facility. We are also indebted to the FORTE operation team, led by Diane Roussel-Dupre and Phil Klingner, for constant support in acquiring and working with FORTE data. We are especially grateful to Charley Rhodes and Daniel Holden, who designed the FORTE antenna, for numerous discussions on the performance of the antenna. This work was performed at the Los Alamos National Laboratory under the auspices of the U.S. Department of Energy.

## References

- Budden, K.G., *The Propagation of Radio Waves*, Cambridge Univ. Press, New York, 1985.
- Davies, K., Recent progress in satellite radio beacon studies with particular emphasis on the ATS-6 Radio Beacon Experiment, *Space Sci. Rev.*, 25, 357-430, 1980.
- Davies, K., *Ionospheric Radio*, Peter Peregrinus, Ltd., London, 1990.
- Farley, D.T., Early incoherent scatter observations at Jicamarca, *J. Atmos. Terr. Phys.*, 53, 665-675, 1991.
- Ho, C.M., B.D. Wilson, A.J. Mannucci, U.J. Lindqwister, and D.N. Yuan, A comparative study of ionospheric total electron content measurements using global ionospheric maps of GPS, TOPEX radar, and the Bent model, *Radio Sci.*, 32(4), 1499-1512, 1997.
- Holden, D.N., C.P. Munson, and J.C. Devenport, Satellite observations of transionospheric pulse pairs, *Geophys. Res. Lett.*, 22(8), 889-892, 1995.
- Jacobson, A.R., and X.M. Shao, Using geomagnetic birefringence to locate sources of impulsive, terrestrial VHF signals detected by satellites on orbit, *Radio Sci.*, 36(4), 671-680, 2001.
- Jacobson, A.R., S.O. Knox, R. Franz, and D.C. Enemark, FORTE observations of lightning radio-frequency signatures: Capabilities and basic results, *Radio Sci.*, 34(2), 337-354, 1999.
- Kraus, J.D., *Radio Astronomy*, Cygnus-Quasar Books, Powell Ohio, 1986.
- Langel, R.A., International Geomagnetic Reference Field: The 6th generation, *J. Geomag. Geoelectr.* 44(9), 679-707, 1992.
- Massey, R.S., S.O. Knox, R.C. Franz, D.N. Holden, and C.T. Rhodes, Measurements of transionospheric radio propagation parameters using the FORTE satellite, *Radio Sci.*, 33(6), 1739-1753, 1998.
- Massey, R. S., and D. N. Holden, phenomenology of transionospheric pulse pairs, *Radio Sci.*, 30(5), 1645-1659, 1995.
- A. R. Jacobson and X.-M. Shao, Space and Atmospheric Sciences Group, NIS-1, MS D466, Los Alamos National Laboratory, Los Alamos, NM 87545, USA. (xshao@lanl.gov)

(Received December 27, 2000; revised July 10, 2001; accepted July 10, 2001.)